JOURNAL OF
APPLIED
CRYSTALLOGRAPHY

Volume 49 (2016)

Supporting information for article:

FAULTS: a program for refinement of structures with extended defects

Montse Casas-Cabanas, Marine Reynaud, Jokin Rikarte, Pavel Horbach and Juan Rodríguez-Carvajal

SUPPLEMENTARY INFORMATION
FAULTS: a program for refinement of structures with extended defects

Montse Casas-Cabanas[a,*], Marine Reynaud[a], Jokin Rikarte[a], Pavel Horbach[b,c] and Juan Rodríguez-Carvajal[b,*]

[a] CIC Energigune, Parque Técnologico de Álava, Albert Einstein 48, 01510 Miñano (Spain)

[b] Institut Laue Languevin, 71 avenue des Martyrs, 38000 Grenoble (France)

[c] Institute for Metal Physics, National Academy of Science, 36 Vernadsky Blvd., 03680, Kiev (Ukraine)

* Correspondence e-mails: mcasas@cicenergigune.com, jrc@ill.eu

1. $Li_{\varepsilon}Ni_{1.02}O_2$ example

Figure SI 1: a) Illustration of the structural model used as starting model for the FAULTS refinement of the simulated pattern of $Li_{\varepsilon}Ni_{1.02}O_2$. b) Comparison between the pattern of the starting model (blue) and the simulated pattern of $Li_{\varepsilon}Ni_{1.02}O_2$ (red) to be refined with FAULTS.

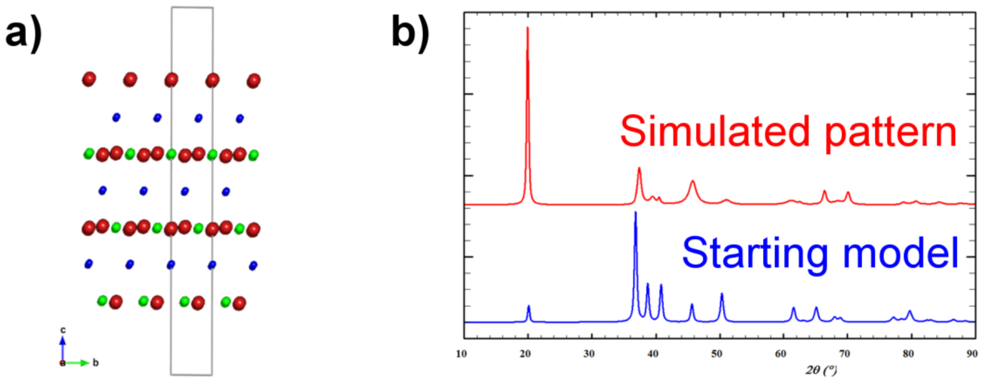

2. MnO_2 example

Figure SI 2: Conventional Rietveld refinement of the XRD pattern of the MnO_2 sample starting from the *pyrolusite* structure and using spherical harmonics to model an anisotropic size broadening. Some of the reflections are not or badly indexed, and their intensities and broadening are poorly simulated.

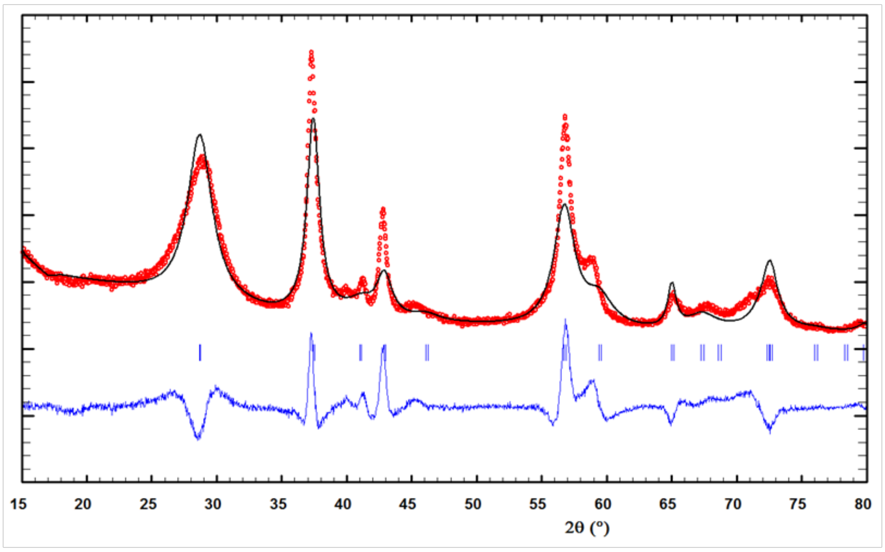

Table SI 1: Structural description of the *pyrolusite* and *ramsdellite* elements used as the starting model for the FAULTS refinement of MnO_2.

		Cell			
a' = 4.4041 Å		*b'* = 2.8765 Å		*c'* = 4.4041 Å	
α = 90º		β = 90º		γ = 90º	
		***Pyrolusite*-type layers**			
	Atom	***x/a***	***y/b***	***z/c***	**Occupancy**
Layer r1	Mn^{IV+} 101	0	0	0	1.0
	O^{II-} 121	0.3046	0	0.3046	1.0
	O^{II-} 122	0.6954	0	-0.3046	1.0
	O^{II-} 141	0.8046	0	0.1954	1.0
	O^{II-} 142	0.1954	0	-0.1954	1.0
Layer r2	Mn^{IV+} 201	½	½	0	1.0
		***Ramsdellite*-type layers**			
	Atom	***x/a***	***y/b***	***z/c***	**Occupancy**
Layer R1	Mn^{IV+} 301	0.0258	¾	0.2805	1.0
	Mn^{IV+} 302	0.9742	¼	-0.2805	1.0
	O^{II-} 321	0.2162	¼	0.0726	1.0
	O^{II-} 322	0.7838	¾	-0.0726	1.0
	O^{II-} 341	0.3001	¾	0.5887	1.0
	O^{II-} 342	0.6799	¼	-0.5887	1.0
	O^{II-} 361	0.8201	¼	0.4641	1.0
	O^{II-} 362	0.1799	¾	-0.4641	1.0
Layer R2	Mn^{IV+} 401	0.4742	¾	0.2805	1.0
	Mn^{IV+} 402	0.5258	¼	-0.2805	1.0
	O^{II-} 421	0.2838	¼	0.0726	1.0
	O^{II-} 422	0.7162	¾	-0.0726	1.0
		Transition vectors			
	Transition	***x/a***	***y/b***	***z/c***	**Type**
From layer r1	r1 → r1	-	-	-	forbidden
	r1 → r2	0	0	½	*pyrolusite*
	r1 → R1	-	-	-	forbidden
	r1 → R2	0	¼	0.7805	De Wolff defect
From layer r2	r2 → r1	0	0	½	*pyrolusite*
	r2 → r2	-	-	-	forbidden
	r2 → R1	0	-¼	0.7805	De Wolff defect
	r2 → R2	-	-	-	forbidden
From layer R1	R1 → r1	-	-	-	forbidden
	R1 → r2	0	-¼	0.7805	De Wolff defect
	R1 → R1	-	-	-	forbidden
	R1 → R2	0	0	1.0528	*ramsdellite*
From layer R2	R2 → r1	0	¼	0.7805	De Wolff defect
	R2 → r2	-	-	-	forbidden
	R2 → R1	0	0	1.0528	*ramsdellite*
	R2 → R2	-	-	-	forbidden

Figure SI 3: Layer description used in the FAULTS refinement of MnO_2.

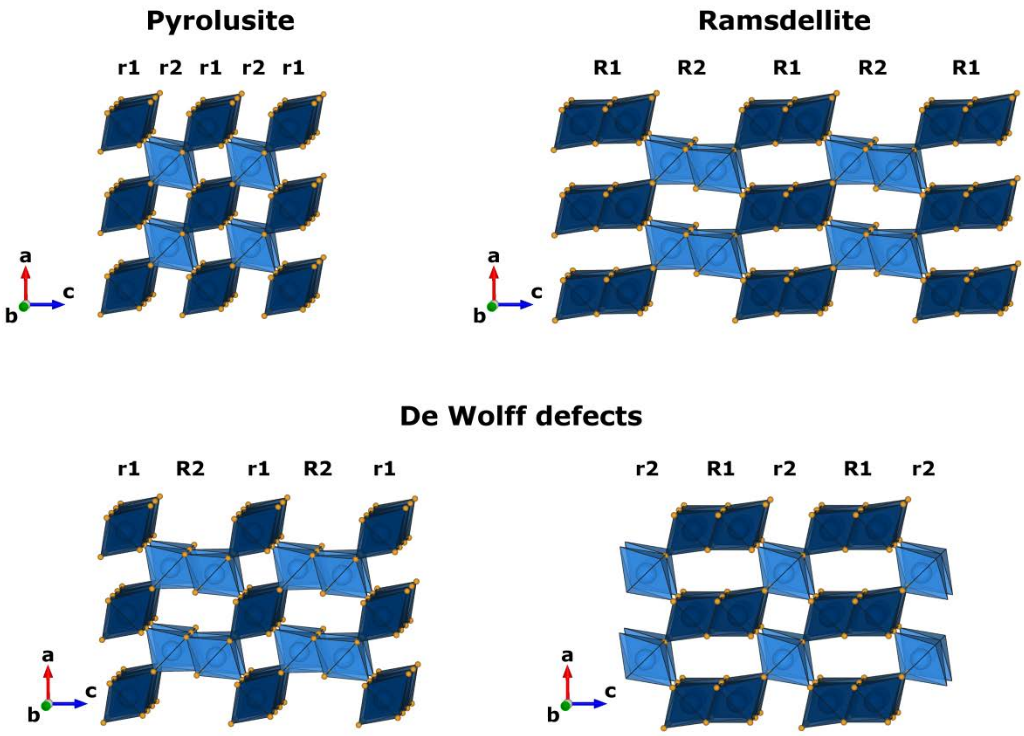

Layer stacking probabilities and stacking models

For the sake of comparison, we have employed the same notations and statistical tools as proposed by Chabre and Pannetier (Chabre & Pannetier, 1995) to describe the sequence of the two kinds of layers:

- P_r and P_R are the respective fractions of single (*rutile*-type = *pyrolusite*-type) and double (*ramsdellite*-type) chain slabs in a given sample. Then, we have the following equality:

$$P_r + P_R = 1$$

- $P_{r \cdot r}$ and $P_{R \cdot r}$ are the probabilities of occurrence of a *rutile* (*pyrolusite*) chain following a *rutile* chain r and a *ramsdellite* chain R, respectively. In the same way, $P_{r \cdot R}$ and $P_{R \cdot R}$ are the probabilities of occurrence of a *ramsdellite* chain R following a *rutile* chain r and a *ramsdellite* chain R, respectively. One can write the following equations:

$$P_{r \cdot r} + P_{r \cdot R} = 1 \quad \text{and} \quad P_{R \cdot r} + P_{R \cdot R} = 1$$

  and one can deduce that:

$$P_r = P_r \cdot P_{r \cdot r} + P_R \cdot P_{R \cdot r} \quad \text{and} \quad P_r = \frac{1 - P_{R \cdot R}}{2 - P_{r \cdot r} - P_{R \cdot R}}$$

$$P_R = P_r \cdot P_{r \cdot R} + P_R \cdot P_{R \cdot R} \quad \text{and} \quad P_R = \frac{1 - P_{r \cdot r}}{2 - P_{r \cdot r} - P_{R \cdot R}}$$

- P_{rR} is the probability of finding a rR or Rr pair at any position in the crystal:

$$P_{rR} = P_{Rr} = P_r \cdot P_{r \cdot R} = P_R \cdot P_{R \cdot r}$$

From the structural model presented in Table SI 1, we simulated the XRD patterns of different models of stacking, which are described below.

1/ <u>Model 1: "Random sequence"</u>

In the first stacking model explored we used a recursive sequence of layers in which the occurrence of a layer does not depend on the previous layer. This model, called "Random sequence" by Chabre and Pannetier (Chabre & Pannetier, 1995), is therefore defined by the following equations:

$$P_{r \cdot r} = P_{R \cdot r} = P_r \ \text{ and } \ P_{R \cdot R} = P_{r \cdot R} = P_R \ \text{ with } P_r = 1 - P_R$$

where P_r and P_R are the respective amount of *pyrolusite* layers and *ramsdellite* layers in the sample.

The stacking rules for this model can be represented with the following chart:

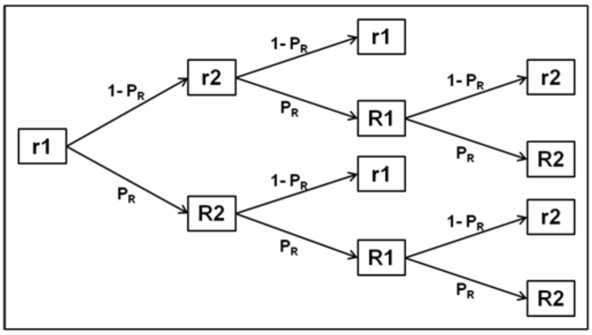

Figure SI 4 shows the evolution of the simulated XRD patterns when varying the value P_R from 0 to 100%. This figure is very comparable with the results obtained by Charbre and Pannetier (Chabre & Pannetier, 1995) with the program DIFFaX (Treacy et al., 1991a). The patterns obtained for P_R = 0% and P_R = 100% correspond to the ideal *pyrolusite* and *ramsdellite* structures, respectively. As the value of P_R increases, we observe a progressive broadening and vanishing of some reflections of the *pyrosulite* (*e.g.*, $(101)_r$ at d ≈ 3.11 Å) while other reflections corresponding to the *ramsdellite* progressively appear and get narrower (*e.g.*, $(101)_R$ at d ≈ 4.06 Å, $(103)_R$ at d ≈ 2.55 Å, $(111)_R$ at d ≈ 2.34 Å, $(113)_R$ at d ≈ 1.90 Å). Note also that in the meantime other reflections do not broaden but only progressively shift their position to go from one structure to the other (*e.g.*, $(011)_r \equiv (012)_R$ at d ≈ 2.41-2.43 Å, $(112)_r \equiv (212)_R$ at d ≈ 1.63-1.66 Å, $(202)_r \equiv (204)_R$ at d ≈ 1.56-1.62 Å).

Figure SI 4: Evolution of the simulated XRD patterns of the intergrowth of *pyrolusite* and *ramsdellite* layers when varying the amount of *ramsdellite* elements P_R from 0 to 100% in the Model 1: “Random sequence”.

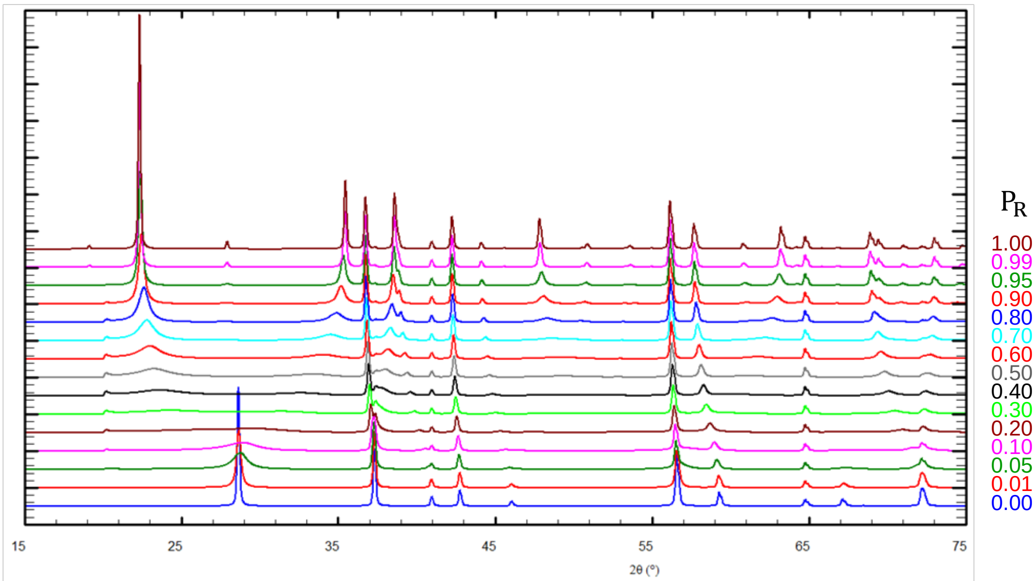

2/ **Model 2 : Segregated sequence**

Conversely to the first model, in the second model, the probability of occurrence of a layer depends on the previous one. We defined P_F the probability of the layer of a given structure type (*pyrolusite* or *ramsdellite*) to be followed by a layer of the other structure:

$$P_{r\cdot R} = P_{R\cdot r} = P_F \quad \text{and thus} \quad P_{r\cdot r} = P_{R\cdot R} = 1 - P_F$$

which can be illustrated by the following chart:

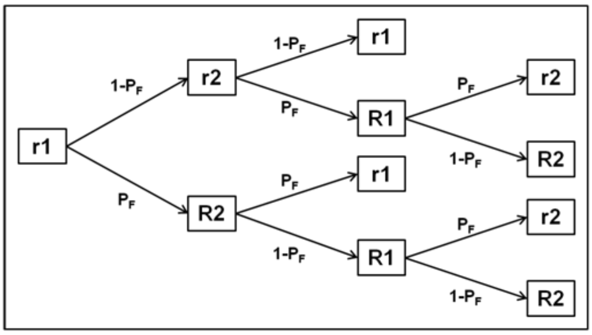

The evolution of the XRD patterns obtained when varying the value of P_F from 0 to 100% are showed in Figure SI 5. The very first pattern ($P_F = 0.0$) is the XRD pattern of the *pyrolusite* structure. The following five patterns ($0.01 \leq P_F \leq 0.3$) correspond to a total or partial segregation between *pyrolusite* and *ramsdellite* domains. As the value of P_F increases, these domains are progressively intermixed, and the structure obtained when $P_F = 100\ \%$ corresponds to the regular alternation of *pyrolusite* and *ramsdellite* layers to produce the ordered sequence r–R–r–R–r–R–…

Figure SI 5: Evolution of the simulated XRD patterns of the intergrowth of *pyrolusite* and *ramsdellite* layers when varying the amount of *ramsdellite* elements P_F from 0 to 100% in the Model 2: Segregated sequence.

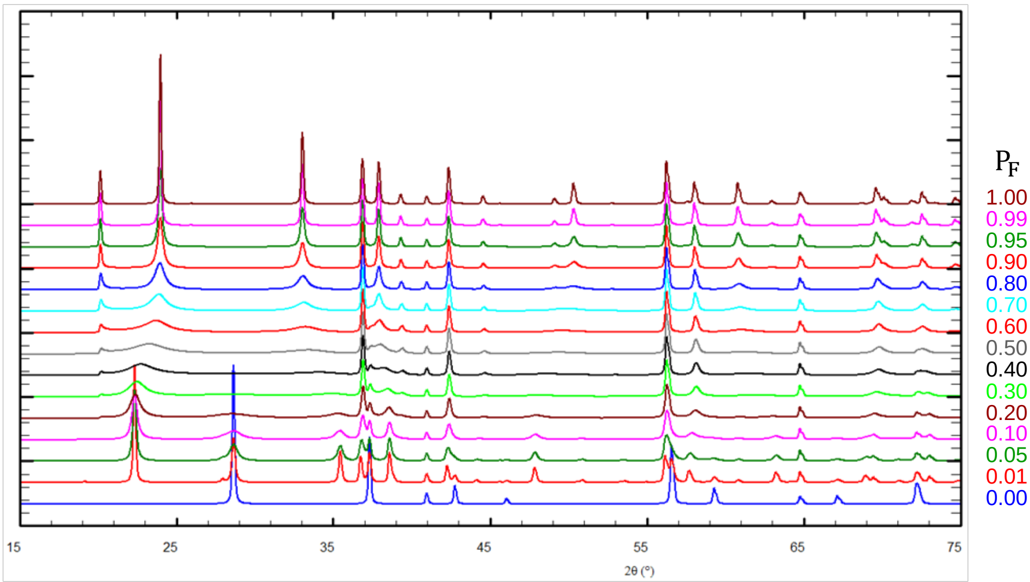

3/ <u>Model 3: “Ordered sequence #1”</u>

The third model corresponds to one example of the “ordered sequences” described by Chabre and Pannetier (Chabre & Pannetier, 1995), in which the probability of occurrence of a RR pair is negligible ($P_{RR} \approx 0$). Therefore this model follows the stacking rule:

$$P_{R \cdot r} = 1 - P_{R \cdot R} = 99.99\%$$

The value of $P_{r \cdot R}$ was then varied from 0 to 100%, so that to vary the amount of *ramsdellite* motif (P_R) from 0 to 50%. The stacking of this model can therefore be illustrated by the following chart:

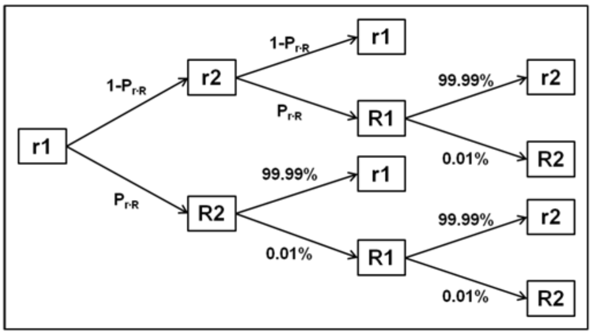

The resulting simulated patterns are shown in Figure SI 6. The pattern calculated for $P_{r \cdot R} = 0$ corresponds to the *pyrolusite* structure, while the one obtained when $P_{r \cdot R} = 100$ % is that of the hypothetical structure of the regular sequence r–R–r–R–r–R–….. As the value of $P_{r \cdot R}$ increases, some peaks split and the diverge from their original position (*e.g.*, $(101)_r$ at d ≈ 3.11 Å, $(011)_r$ at d ≈ 2.41 Å, $(002)_r$ at d ≈ 2.20 Å). Moreover, the introduction of *ramsdellite* motifs into the *pyrolusite* lattice goes with the appearance of a tiny reflection at d ≈ 4.40 Å ($2\theta_{\lambda=Cu} \approx 20°$), which is subject to a kind of Warren fall and whose intensity increases and shape becomes more symmetric until forms the perfectly ordered phase r-R-r-R-r. One can note that this feature was also present in Model 2: Segregated sequence (Figure SI 5), although is less obvious.

Figure SI 6: Evolution of the simulated XRD patterns of the intergrowth of *pyrolusite* and *ramsdellite* layers when varying the probability of having a *ramsdellite* elements after a *pyrolusite* one $P_{r \cdot R}$ from 0 to 100% in the Model 3: Ordered sequence #1.

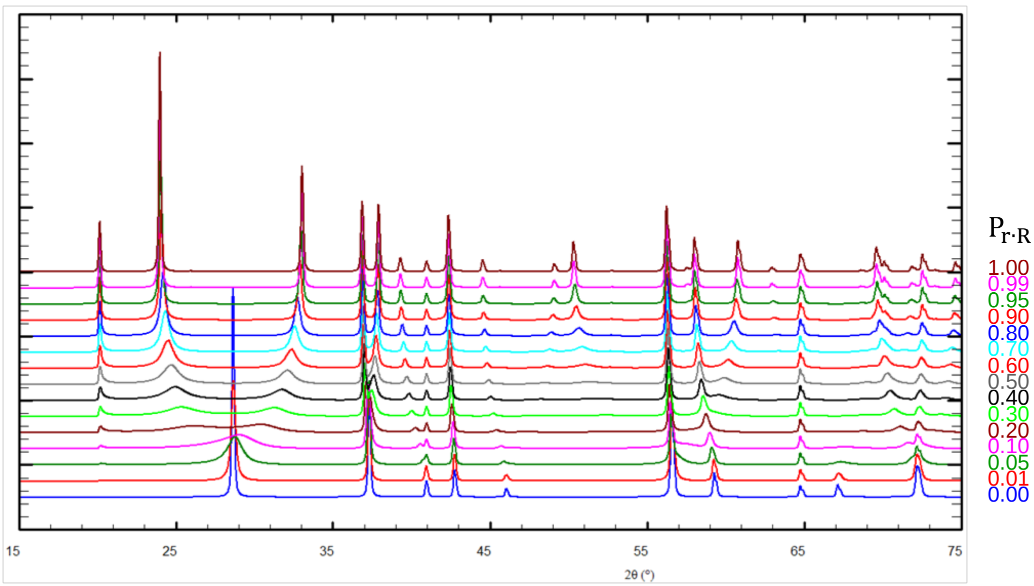

4/ <u>**Model 4: "Ordered sequence #2"**</u>

The fourth model is the opposite example of the "ordered sequence" described by Chabre and Pannetier (Chabre & Pannetier, 1995), and is characterized by the negligible probability of occurring a rr pair in the *ramsdellite* framework ($P_{rr} \approx 0$). It is therefore defined by the following equation:

$$P_{r \cdot R} = 1 - P_{r \cdot r} = 99.99\%$$

Similarly to the previous model, the value of $P_{R \cdot r}$ was varied from 0 to 100%, so that to vary the amount of *pyrolusite* motif in the structure (P_r) from 0 to 50%. The stacking of this model can therefore be illustrated by the following chart:

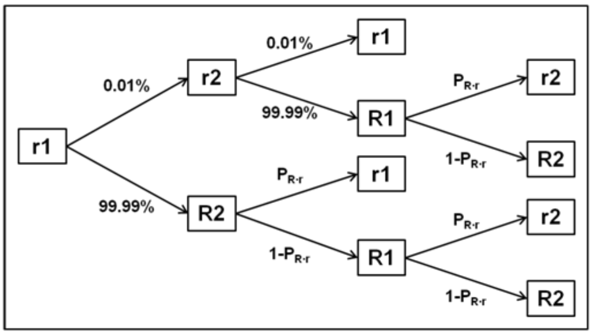

The resulting simulated patterns are shown in Figure SI 7. In this case, the first pattern corresponds to that of the *ramsdellite* structure, and, again, the structure obtained when $P_{R \cdot r}$ = 100 % is the regular alternation of the two kinds of chains r–R–r–R–r–R–…

Figure SI 7: Evolution of the simulated XRD patterns of the intergrowth of *pyrolusite* and *ramsdellite* layers when varying the probability of having a *pyrolusite* elements after a *ramsdellite* one $P_{R \cdot r}$ from 0 to 100% in the Model 4: Ordered sequence #2.

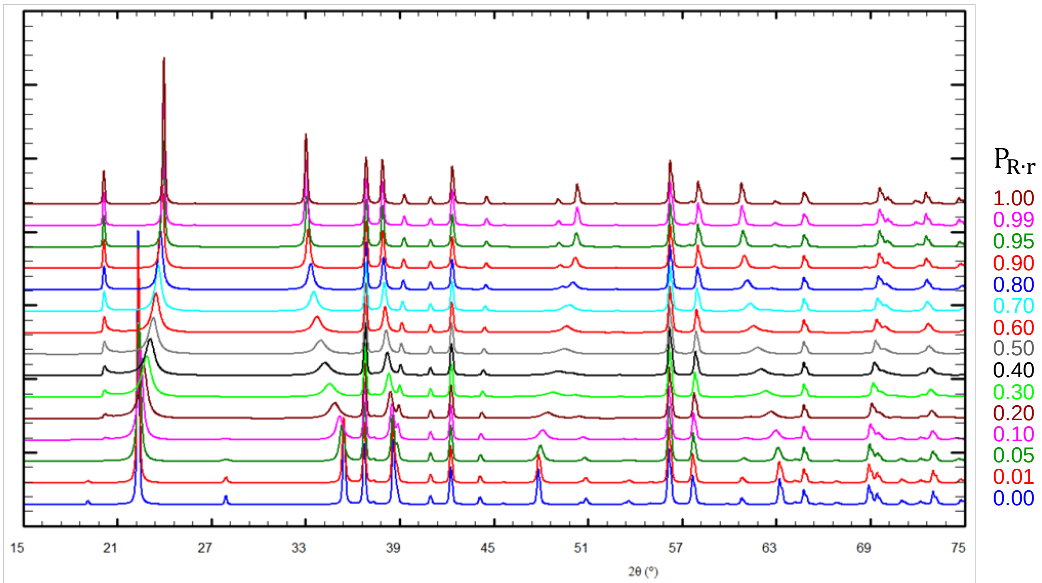

5/ Intermediate models

In the fifth and sixth models, we fixed the probability of having a *ramsdellite* layer after a *rutile* one ($P_{r\cdot R}$) to 5 and 10 %, respectively, and we followed the evolution of the patterns of while varying the probability of maintaining a *ramsdellite* domain after a *ramsdellite* slab ($0 \leq P_{R\cdot R} \leq 100\%$):

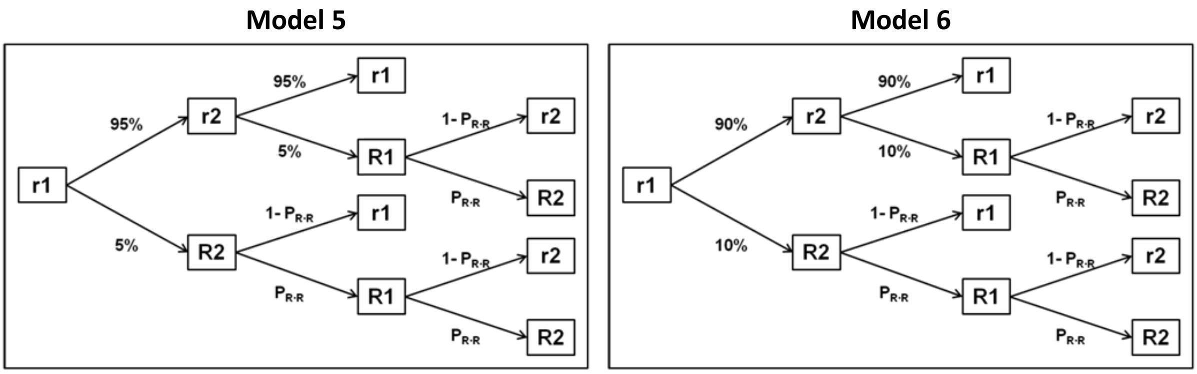

These models permit to simulate the effect of how extended are the domains of *ramsdellite* (one or several *ramsdellite* layers). The results of these simulations are presented in Figure SI 8and Figure SI 9, respectively. The diagrams obtained for $P_{R\cdot R}$ = 0% and $P_{R\cdot R}$ = 100% are close to the ones of *pyrolusite* and *ramsdellite*, respectively. These figures show that the XRD patterns of the intergrowth of *pyrolusite* and *ramsdellite* do not suffer from much modification when varying $P_{R\cdot R}$ between 0 and 50 %, except that the main reflection $(011)_r$ at d ≈ 2.41 Å is progressively split in two peaks as the $P_{R\cdot R}$ increases. This means that for *pyrolusite* structures containing low content of *ramsdellite* inclusions, it is difficult to decipher if these inclusions are of the form of single layer of *ramsdellite* or larger domains of *ramsdellite* (several layers).

Figure SI 8: Evolution of the simulated XRD patterns of the intergrowth of *pyrolusite* and *ramsdellite* layers when varying the probability of having a *ramsdellite* elements after a *ramsdellite* one $P_{R\cdot R}$ from 0 to 100% in the Model 5, while the probability of having a *ramsdellite* layer after a *rutile* one ($P_{r\cdot R}$) is fixed to 5 %.

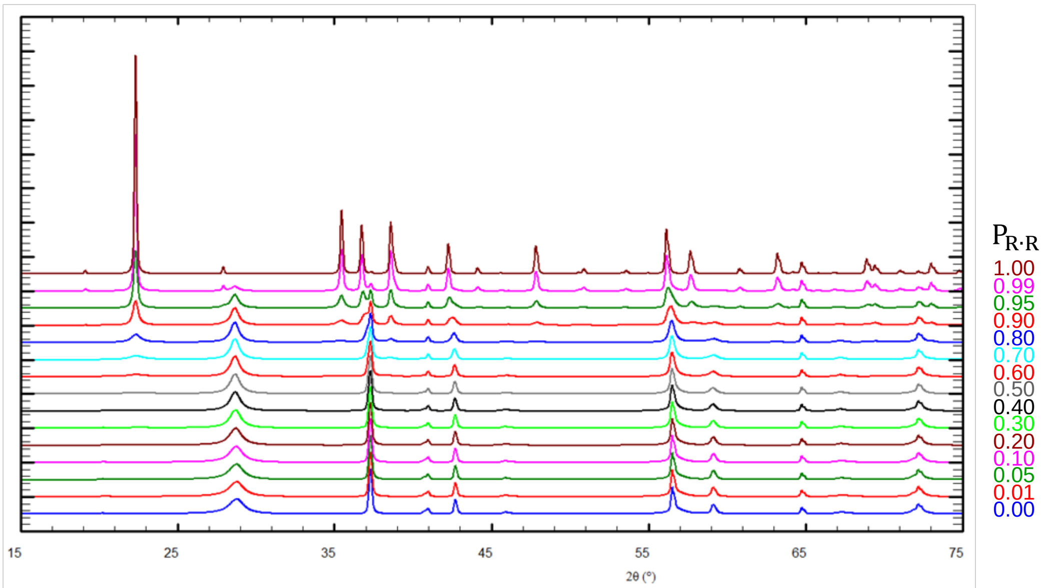

Figure SI 9: Evolution of the simulated XRD patterns of the intergrowth of *pyrolusite* and *ramsdellite* layers when varying the probability of having a *ramsdellite* elements after a *ramsdellite* $P_{R \cdot R}$ from 0 to 100% in the Model 6, while the probability of having a *ramsdellite* layer after a *rutile* one ($P_{r \cdot R}$) is fixed to 10 %.

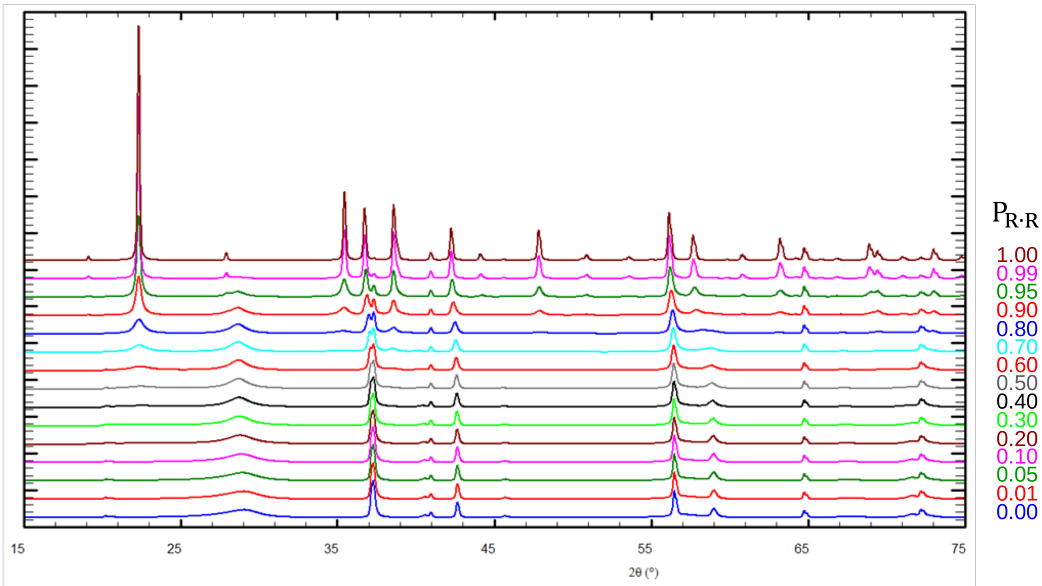

Table SI 2: Selected distances of the refined model for the MnO_2 sample

***Pyrolusite*-type stacking**			
r1–r2–r1			
Mn^{IV+} 101 – O^{II-} 121	1.85(5)	Mn^{IV+} 201 – O^{II-} 121	1.93(3)
Mn^{IV+} 101 – O^{II-} 122	1.85(5)	Mn^{IV+} 201 – O^{II-} 121	1.93(3)
Mn^{IV+} 101 – O^{II-} 141	1.88(3)	Mn^{IV+} 201 – O^{II-} 122	1.93(3)
Mn^{IV+} 101 – O^{II-} 141	1.88(3)	Mn^{IV+} 201 – O^{II-} 122	1.93(3)
Mn^{IV+} 101 – O^{II-} 142	1.88(3)	Mn^{IV+} 201 – O^{II-} 141	1.90(5)
Mn^{IV+} 101 – O^{II-} 142	1.88(3)	Mn^{IV+} 201 – O^{II-} 142	1.90(5)
***Ramsdellite*-type stacking**			
R1–R2–R1			
Mn^{IV+} 301 – O^{II-} 321	2.14(5)	Mn^{IV+} 401 – O^{II-} 421	2.26(5)
Mn^{IV+} 301 – O^{II-} 321	2.14(5)	Mn^{IV+} 401 – O^{II-} 421	2.26(5)
Mn^{IV+} 301 – O^{II-} 322	1.82(7)	Mn^{IV+} 401 – O^{II-} 422	1.88(7)
Mn^{IV+} 301 – O^{II-} 341	1.97(7)	Mn^{IV+} 401 – O^{II-} 342	1.82(4)
Mn^{IV+} 301 – O^{II-} 361	1.96(5)	Mn^{IV+} 401 – O^{II-} 342	1.82(4)
Mn^{IV+} 301 – O^{II-} 361	1.96(5)	Mn^{IV+} 401 – O^{II-} 362	1.98(7)
Mn^{IV+} 302 – O^{II-} 321	1.82(7)	Mn^{IV+} 402 – O^{II-} 421	1.88(7)
Mn^{IV+} 302 – O^{II-} 322	2.14(5)	Mn^{IV+} 402 – O^{II-} 422	2.26(5)
Mn^{IV+} 302 – O^{II-} 322	2.14(5)	Mn^{IV+} 402 – O^{II-} 422	2.26(5)
Mn^{IV+} 302 – O^{II-} 342	1.97(7)	Mn^{IV+} 402 – O^{II-} 341	1.82(4)
Mn^{IV+} 302 – O^{II-} 362	1.96(5)	Mn^{IV+} 402 – O^{II-} 341	1.82(4)
Mn^{IV+} 302 – O^{II-} 362	1.96(5)	Mn^{IV+} 402 – O^{II-} 361	1.98(7)
De Wolff defects stacking			
r1–R2–r1		**r2–R1–r2**	
Mn^{IV+} 101 – O^{II-} 121	1.85(5)	Mn^{IV+} 201 – O^{II-} 341	1.84(3)
Mn^{IV+} 101 – O^{II-} 122	1.85(5)	Mn^{IV+} 201 – O^{II-} 341	1.84(3)
Mn^{IV+} 101 – O^{II-} 141	1.88(3)	Mn^{IV+} 201 – O^{II-} 361	1.98(5)
Mn^{IV+} 101 – O^{II-} 141	1.88(3)	Mn^{IV+} 201 – O^{II-} 342	1.84(3)
Mn^{IV+} 101 – O^{II-} 142	1.88(3)	Mn^{IV+} 201 – O^{II-} 342	1.84(3)
Mn^{IV+} 101 – O^{II-} 142	1.88(3)	Mn^{IV+} 201 – O^{II-} 362	1.98(5)
Mn^{IV+} 401 – O^{II-} 421	2.26(5)	Mn^{IV+} 301 – O^{II-} 321	2.14(5)
Mn^{IV+} 401 – O^{II-} 421	2.26(5)	Mn^{IV+} 301 – O^{II-} 321	2.14(5)
Mn^{IV+} 401 – O^{II-} 422	1.88(7)	Mn^{IV+} 301 – O^{II-} 322	1.82(7)
Mn^{IV+} 401 – O^{II-} 122	1.90(5)	Mn^{IV+} 301 – O^{II-} 341	1.97(7)
Mn^{IV+} 401 – O^{II-} 122	1.90(5)	Mn^{IV+} 301 – O^{II-} 361	1.96(5)
Mn^{IV+} 401 – O^{II-} 142	1.93(7)	Mn^{IV+} 301 – O^{II-} 361	1.96(5)
Mn^{IV+} 402 – O^{II-} 421	1.88(7)	Mn^{IV+} 302 – O^{II-} 321	1.82(7)
Mn^{IV+} 402 – O^{II-} 422	2.26(5)	Mn^{IV+} 302 – O^{II-} 322	2.14(5)
Mn^{IV+} 402 – O^{II-} 422	2.26(5)	Mn^{IV+} 302 – O^{II-} 322	2.14(5)
Mn^{IV+} 402 – O^{II-} 121	1.90(5)	Mn^{IV+} 302 – O^{II-} 342	1.97(7)
Mn^{IV+} 402 – O^{II-} 121	1.90(5)	Mn^{IV+} 302 – O^{II-} 362	1.96(5)
Mn^{IV+} 402 – O^{II-} 141	1.93(7)	Mn^{IV+} 302 – O^{II-} 362	1.96(5)

Figure SI 10: Results of the FAULTS refinement of the MnO_2 sample when refining the layer width instead of the isotropic broadening parameters Dl and Dg. Remark that the reflection $(002)_r$ at d ≈ 2.24 Å ($2\theta_{Cu}$ ≈ 40.0°) is not well modelled.

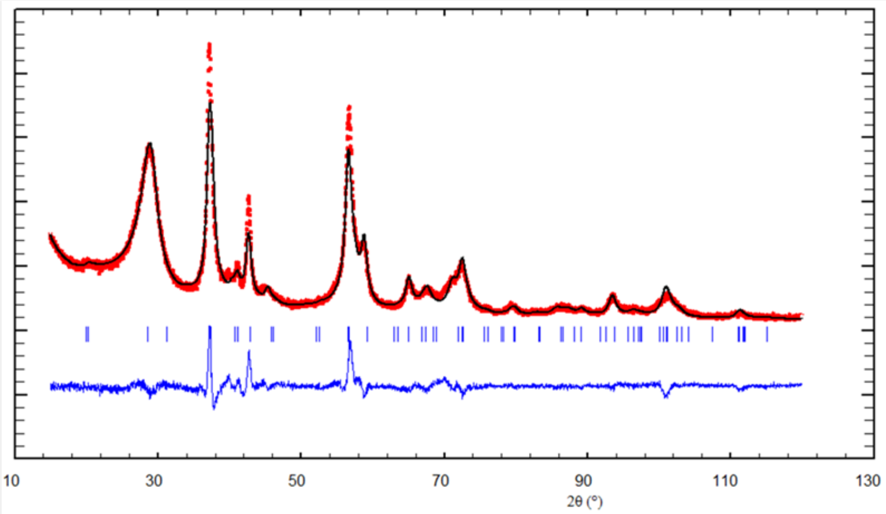

Figure SI 11: Evolution of the XRD pattern of the *pyrolusite* with the presence of twinning (twin plane (011), from ideal *pyrolusite* (P_t = 0.0) to fully twinned *pyrolusite* (P_t = 1.0).

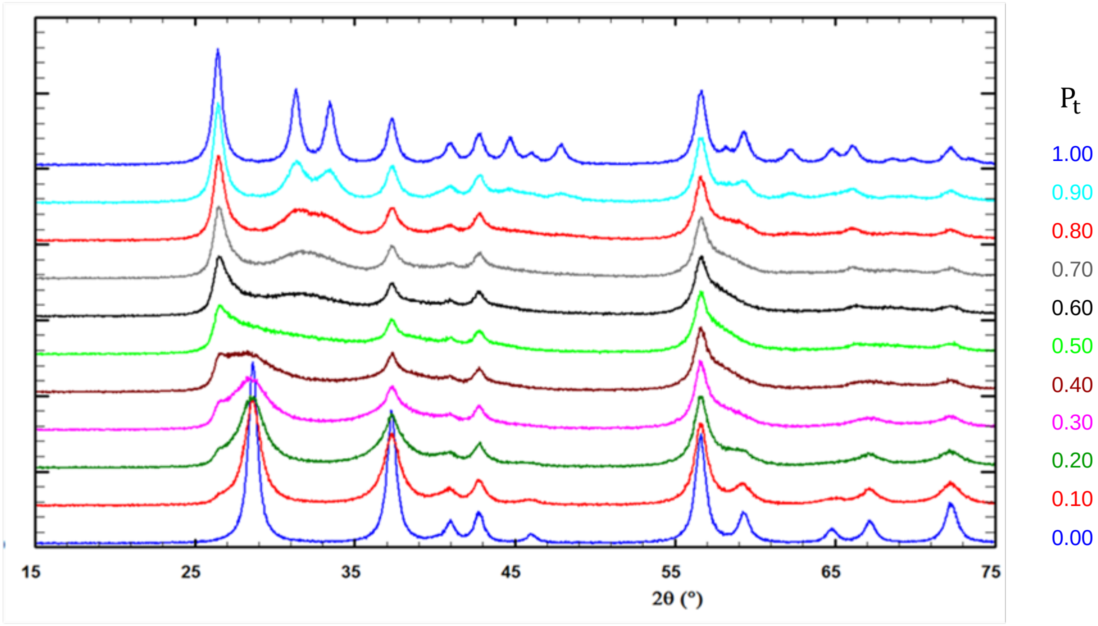

To simulate the effect of twinning in the *pyrolusite* lattice along (011), new layers were defined so that to have the staking direction perpendicular to the twinning place. The structural model used in FAULTS is described in Table SI 3 and an illustration of a possible twinning is shown in Figure SI 12.

Table SI 3: Structural model used to described twinned *pyrolusite* (twin plane (011).

Cell					
a'' = 4.4041 Å α = 90º		b'' = 5.2603 Å β = 90º		c'' = 4.81664 Å γ = 90º	
Layers					
	Atom	***x*/*a***	***y*/*b***	***z*/*c***	**Occupancy**
Layer T1 = T3	Mn^{IV+} 11	0	0	0	1.0
	Mn^{IV+} 12	½	½	0	1.0
	O^{II-} 111	¼	¼	1/6	1.0
	O^{II-} 112	¼	½	-1/3	1.0
	O^{II-} 121	¾	½	1/3	1.0
	O^{II-} 122	¾	¾	-1/6	1.0
	O^{II-} 131	¾	¼	-1/6	1.0
	O^{II-} 132	¾	0	1/3	1.0
	O^{II-} 141	¼	0	-1/3	1.0
	O^{II-} 142	¼	¾	1/6	1.0
Layer T2 = T4	Mn^{IV+} 21	0	0	0	1.0
	Mn^{IV+} 22	½	½	0	1.0

Transition vectors						
	Transition	***x*/*a***	***y*/*b***	***z*/*c***	**Probability**	**Type**
From layer T1	T1 → T1	-	-	-	0	forbidden
	T1 → T2	0	-0.299	½	$1-P_t$	no twinning
	T1 → T3	-	-	-	0	forbidden
	T1 → T4	0	0.299	½	P_t	twinning
From layeT T2	T2 → T1	0	-0.299	½	$1-P_t$	no twinning
	T2 → T2	-	-	-	0	forbidden
	T2 → T3	0	0.201	½	P_t	twinning
	T2 → T4	-	-	-	0	forbidden
From layeT T3	T3 → T1	-	-	-	0	forbidden
	T3 → T2	0	-0.299	½	P_t	twinning
	T3 → T3	-	-	-	0	forbidden
	T3 → T4	0	0.299	½	$1-P_t$	no twinning
From layeT T4	T4 → T1	0	-0.201	½	P_t	twinning
	T4 → T2	-	-	-	0	forbidden
	T4 → T3	0	0.299	½	$1-P_t$	no twinning
	T4 → T4	-	-	-	0	forbidden

Figure SI 12: Illustration of a possible twinning of the *pyrolusite* along the twin plane (011).